Journal of Inorganic and General Chemistry
ZAAC
Zeitschrift für anorganische und allgemeine Chemie
www.zaac.wiley-vch.de
RESEARCH ARTICLE

DOI: 10.1002/zaac.202200171

Phase Control in the Modulated Self-Assembly of Lanthanide MOFs of a Flexible Tetratopic Bis-Amide Linker

Alexander J. R. Thom,[a] Emma Regincós Martí,[a] Ignas Pakamorė,[a] Claire Wilson,[a] and Ross S. Forgan*[a]

The targeted synthesis of phase-pure metal-organic frameworks (MOFs) is often complicated by the fact that a number of different products can result from the same metal-ligand combination. The self-assembly of lanthanide-based MOFs can be particularly challenging due to the versatile coordination chemistry of the *f*-block allowing for diverse coordination spheres with irregular geometries driven by steric effects. Herein we show that modulated self-assembly – the addition of small molecules to solvothermal synthesis in order to control pH and coordination equilibria – can control phase formation when preparing lanthanide MOFs from the tetratopic bis-(3,5-dicarboxyphenyl)terephthalamide ligand. We report 27 new MOFs, of which 21 are characterised by single crystal X-ray diffraction, that can be categorised into six structure types. The formation of different phases is largely driven by the contraction in ionic radius across the lanthanide series, but we show how careful choice of both solvent and modulator can influence reaction outcome. As an example, phase pure samples of three Gd MOFs of the same ligand can be selected by simply changing the modulator – acetic acid, benzoic acid, or nitric acid – used in closely related syntheses. These results show that modulation can control phase in *f*-block MOFs, just as it can in *d*-block MOFs, and provide design rules for uncovering structural diversity by carefully exploring the chemical parameter space of lanthanide MOFs in single ligand systems.

Introduction

The photo-physics of metal-organic frameworks (MOFs), network solids where metal ions or clusters are connected by organic ligands,[1] has attracted notable attention due to the potential applications of photoactive MOFs as photon upconverters,[2] white light emitting diodes (LEDs),[3] sensors,[4] and bioimaging agents.[5] Of special interest has been the use of lanthanide MOFs (Ln MOFs)[6] that inherit the tuneable, sensitive and well-defined photophysical properties of the lanthanide metal(s) that are enhanced by the antenna effect,[7] making them ideal candidates for use in sensing and as emissive materials in general.[8] Lanthanide coordination chemistry is dominated by ligand sterics rather than ligand field effects, where buried 4*f* orbitals and a lack of structural directionality by the outermost 5*s* orbital contribute to the lack of defined coordination geometries.[9] As such, when assembling coordination polymers, multiple different topologies can typically be accessed from individual metal-ligand combinations.[10] Overcoming this challenge, and fully understanding the synthesis of Ln MOFs, is therefore of the utmost importance for the development of new, applied materials.

The flexible coordination chemistry of the lanthanides means controlling Ln(III) MOF syntheses to reproducibly prepare the same, phase pure material is challenging.[11] Subtle modifications to synthetic conditions, such as changes in solvent, temperature, pH and starting material ratios, therefore present an opportunity to synthesise many new structures.[12] Modulation, the purposeful addition of a compound to influence the crystallinity, particle size, morphology and/or the phase of the resulting MOF,[13] has been shown to exert phase control in MOFs linked by trivalent metals such as Al(III),[14] Fe(III),[15] and Cr(III),[16] but has not been widely investigated in the synthesis of Ln(III) MOFs, with examples limited to morphological control.[17] Previously, we have shown that Y(III), which has closely related coordination chemistry to the lanthanides, can controllably form six different phases with the 2,6-naphthalenedicarboxylate ligand through use of different modulators.[18] Herein, we examine the effect of both the lanthanide contraction[19] and modulation in the self-assembly of a series of Ln(III) MOFs with the tetratopic ligand bis-(3,5-dicarboxyphenyl)terephthalamide (H_4L). By combining a ligand with inherently flexible amide units and a range of different lanthanides, we describe the formation of six predominant phases – GUF-2(Ln), GUF-3(Ln), GUF-4(Ln), GUF-5(Ln), GUF-6(Ln), and GUF-7(Ln) (GUF=Glasgow University Framework) - that are largely dependent on lanthanide ionic radius, in addition to a seventh that has been previously reported.[20] We show multiple examples of modulated syntheses leading to different phases from the same metal-ligand combination – gadolinium versions of three of the new phases can be isolated – suggesting great

[a] *A. J. R. Thom, E. Regincós Martí, I. Pakamorė, C. Wilson, R. S. Forgan*
WestCHEM School of Chemistry, University of Glasgow, Joseph Black Building, University Avenue, Glasgow G12 8QQ, UK
E-mail: Ross.Forgan@glasgow.ac.uk

Supporting information for this article is available on the WWW under https://doi.org/10.1002/zaac.202200171

structural diversity and control is possible through modulated self-assembly of Ln MOFs.

Results and Discussion

Single Crystal Structures

Previously, MOFs with the general formula $[Ln_2(L)_{1.5}(DMF)_4]_n$, where DMF=*N*,*N*-dimethylformamide, have been isolated for Tb(III), through synthesis in 4:1 (*v*/*v*) DMF:H_2O at 75 °C with nitric acid modulation,[20a] and for Dy(III) and Sm(III) in solvothermal syntheses in DMF at 100 °C.[20b] A 5:1:40 Ln:H_4L:HNO_3 stoichiometry was used in the former, and a 2:1 Ln:H_4L ratio in the latter, with 48 hour synthesis times for all. Our initial attempts to prepare lanthanide MOFs from H_4L (prepared by a literature procedure)[21] and lanthanide nitrates involved a stochastic approach to the investigation of the wide chemical parameter space in terms of modulator, solvent, reaction stoichiometry, temperature, etc. It became quickly clear that this approach was not optimal for controllably generating materials, and so to homogenise conditions across the lanthanides, we selected conditions whereby H_4L and the lanthanide nitrate (1:1 ratio) were combined in a 1:1 (*v*/*v*) mixture of *N*,*N*-dimethylformamide (DMF) and water, and heated at 80 °C for 24 hours in the presence of varying equivalents of different modulators, where required. For each material described, precise synthetic conditions are reported in the supporting information, Section S3. MOFs were initially analysed through single crystal X-ray diffraction (SCXRD), and if bulk samples could be obtained, by powder X-ray diffraction (PXRD) and thermogravimetric analysis (TGA).

Some unsuccessful syntheses resulted in recrystallization of the linker as the bis-DMF solvate (Figure 1). Hydrogen bonds form between the formamide oxygen of the DMF molecules and the amide NH moieties of H_4L (N1···O1S = 2.937 (3) Å), while the linkers themselves associate via a conventional carboxylic acid hydrogen bonded dimer (O4···O3 = 2.629 (3) Å) and a hydrogen bond between a carboxylic acid unit and the amide carbonyl (O1···O5 = 2.597 (3) Å). This results in ribbons of H_4L molecules, connected by the carboxylic acid dimer, that hydrogen bond to each other forming two-dimensional sheets with DMF molecules enclosed in vacancies, reminiscent of hydrogen-bonded organic frameworks.[22] These sheets then form offset π-stacks at an interplanar distance of approximately 3.6 Å.

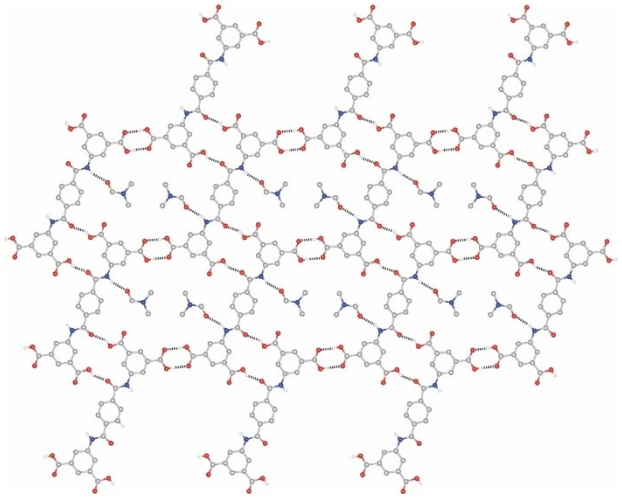

Figure 1. Crystal structure of H_4L·2DMF illustrating the formation of hydrogen bonded two-dimensional sheets. C: grey; O: red; N: blue; H: white. H atoms not involved in hydrogen bonding removed for clarity.

Crystal structures of the first three MOFs in this study, GUF-2(Ln), GUF-3(Ln), and GUF-4(Ln), were obtained for the early lanthanides using crystals isolated from very similar (or indeed identical) reactions. The materials show significant structural similarities, all being two-dimensional MOFs linked by Ln_2 secondary building units (SBUs) with the linker being in the monoprotonated state to allow charge balance, giving the general formula [Ln(HL)(solvent)$_x$]. The MOFs often crystallised together in individual syntheses, making scale-up of phase pure samples highly challenging. The first MOF, GUF-2(Ln), could be crystallised with La(III) and Ce(III) using two equivalents of HNO_3 as a modulator in a 1:1 (*v*/*v*) DMF:H_2O solvent mixture. GUF-2(La) will be described as representative of both MOFs, and crystallises in the triclinic *P*-1 space group with an overall formula of $([La(HL)(H_2O)_4]\cdot\{H_2O\}_2)_n$. A centrosymmetric dimer of nine-coordinate La(III) units with formula $[La_2(\mu_2\text{-}RCOO)_2(RCOO)_2(RCOOH)_2(H_2O)_8]$ is present (Figure 2a), where two carboxylates bridge the dimer in the $\eta_2:\kappa_{1:}\kappa_1$ binding mode (η describes the binding mode of the carboxylate as a whole and κ describes the binding mode of each individual oxygen atom of the carboxylate), two carboxylates coordinate one to each La(III) ion in a bidentate, $\eta_1:\kappa_{1:}\kappa_1$ manner, and two protonated carboxylates coordinate to each La(III) ion in a monodentate $\eta_1:\kappa_{1:}\kappa_0$ motif. The dimer participates in significant outer sphere hydrogen bonding. Within the dimer, a water ligand on one La(III) unit hydrogen bonds to a water ligand on the adjacent La(III) of the dimer (O4W···O3W = 2.941 (6) Å; analogous distances for GUF-2(Ce) are given in the SI, Table S2). One carboxylate unit of HL is unusually both uncoordinated and deprotonated, and enters into a network of outer sphere H-bond interactions (Figure 2a) with an adjacent cluster on the same 2D sheet, to three coordinated water molecules (O2W···O5 = 2.956 (5) Å; O3W···O5 = 2.674 (5) Å; O4W···O6 = 2.905 (5) Å) and the protonated carboxylic acid unit (O3···O6 = 2.500 (5) Å). These dimers connect linker molecules into two-dimensional sheets (Figure 2b) which are two linkers in depth in an offset stacking arrangement around 3.3 Å apart. Hydrogen bonds are formed from the uncoordinated carboxylate unit to a water ligand on an adjacent sheet (O2W···O5′ = 2.866 (4) Å) and from another coordinated water to an amide oxygen (O3W···O10′ = 2.734 (4) Å). These are the only major interactions between the layers in the structure, which themselves are distanced by around 3.5 Å. Infinite channels, which are filled with ordered water molecules, are apparent when the structure is viewed down the crystallographic *a*-axis (Figure 2c). Pairs of these water molecules hydrogen bond to each other and extensively to donors and acceptors on both the linker amide

Journal of Inorganic and General Chemistry
ZAAC
Zeitschrift für anorganische und allgemeine Chemie

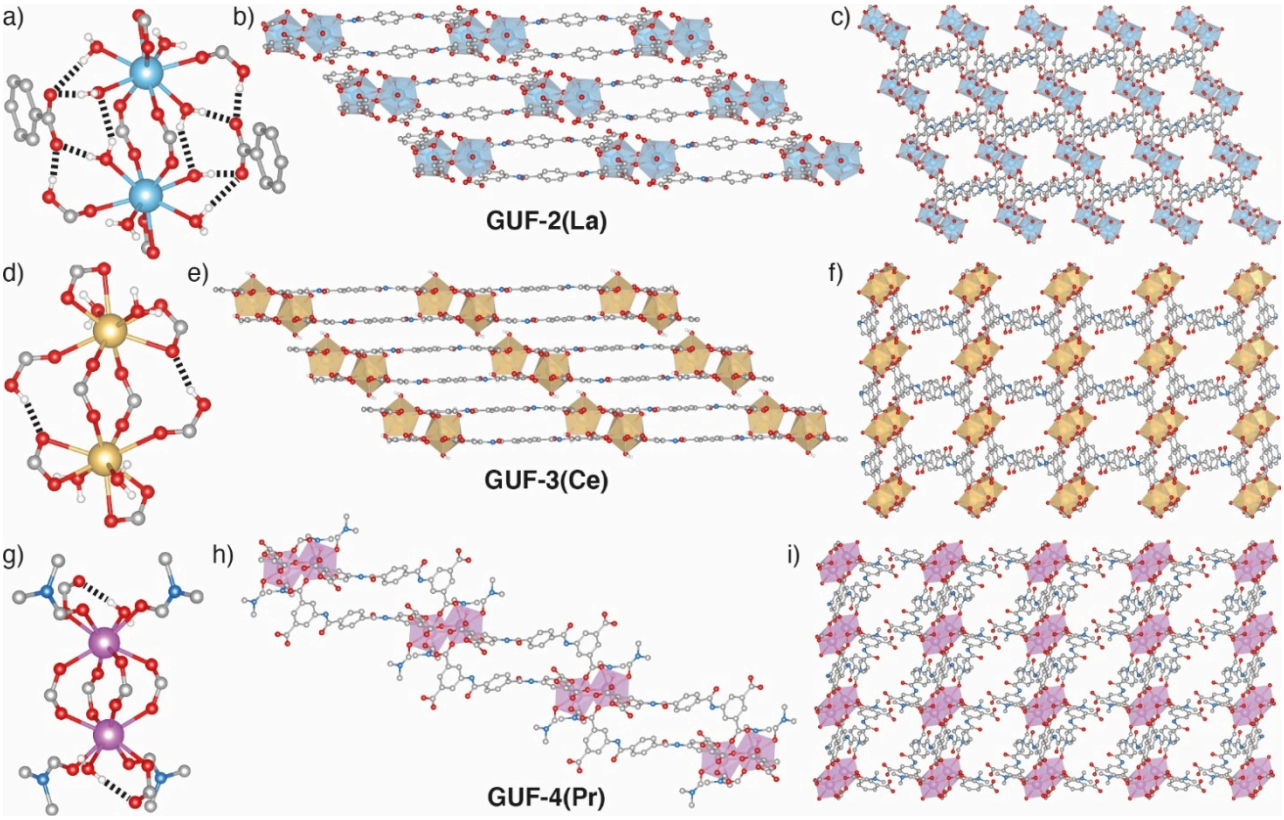

Figure 2. Crystal structure of GUF-2(La). a) Dimeric La(III) SBU showing outer sphere H-bonding. b) Offset stacking of two-dimensional sheets viewed down the crystallographic *b*-axis. c) Packing structure viewed down the crystallographic *a*-axis showing channels (bound water guest molecules removed for clarity). Crystal structure of GUF-3(Ce). d) Dimeric Ce(III) SBU showing outer sphere H-bonding. e) Offset linear stacking of two-dimensional sheets viewed along the crystallographic *a*-axis with inter-dimer H-bonding. f) Stacked sheets viewed down the crystallographic *b*-axis showing solvent-accessible channels. Crystal structure of GUF-4(Pr). g) Dimeric Pr(III) paddlewheel SBU showing outer sphere H-bonding. h) Stepped two-dimensional sheet structure viewed down the crystallographic *a*-axis. i) Packing structure viewed down the crystallographic *c*-axis to show solvent accessible channels. La: light blue; Ce: gold; Pr: pale purple; C: grey; O: red; N: blue; H: white. H atoms removed for clarity other than those involved in outer sphere H-bonding interactions in parts a), d) and g).

groups and at the SBUs (SI, Figure S1). The two-dimensional MOF has **sql** topology with point symbol $\{4^4.6^2\}$ (SI, Figure S2).

The second MOF, GUF-3(Ln), could be crystallised with Ce(III), Pr(III), and Nd(III), using two to four equivalents of HNO_3 as a modulator in a 1:1 (*v*/*v*) DMF:H_2O solvent mixture. GUF-3(Ln) is very closely related to GUF-2(Ln), with the only difference being that while the linker is again monoprotonated, all four carboxylates now coordinate to the Ln_2 SBU, meaning two water ligands per Ln(III) are no longer required to fill the coordination sphere of the nine-coordinate ion, giving an overall formula of $[Ln(HL)(H_2O)_2]_n$. The Ce(III) congener will be described as representative of the series, which crystallises in the triclinic *P*-1 space group, and is again linked by a centrosymmetric nine-coordinate Ce(III) dimer, this time with formula $[Ce_2(\mu_2\text{-}RCOO)_2(RCOO)_4(RCOOH)_2(H_2O)_4]$ (Figure 2d). Two carboxylates bridge the dimer in the $\eta_2{:}\kappa_{1:}\kappa_1$ binding mode, two carboxylates coordinate to each individual Ce(III) ion in a bidentate, $\eta_1{:}\kappa_{1:}\kappa_1$ manner (in contrast to one per Ln(III) ion in GUF-2(Ln)), and two protonated carboxylates coordinate, one to each Ce(III), in a monodentate $\eta_1{:}\kappa_{1:}\kappa_0$ motif, with the OH unit entering into a short hydrogen bond with the oxygen of a bidentate carboxylate on the adjacent Ce(III) (O3···O7 = 2.669 (3) Å; analogous distances for the other members of the series are given in the SI, Table S4). Connection of the clusters by the linker results in a similar two-dimensional sheet structure to GUF-2(Ln). The sheets are two linkers in depth; molecules of HL form offset stacks at an interplanar distance of approximately 3.5 Å. Viewing the structure of GUF-3(Ce) along the crystallographic *a*-axis shows the stacking of these layers, with the second water ligand from each Ce(III) dimer forming bifurcated hydrogen bonds to individual carboxylate oxygen donors on a dimer of an the adjacent sheet (O2W···O5 = 2.921 (3) Å, O2W···O8 = 2.918 (3) Å), bringing each sheet together into an offset stacking arrangement with an inter-sheet spacing of approximately 3.4 Å (Figure 2e). When viewed down the crystallographic *b*-axis (Figure 2f) channels are apparent, into which projects one of the H_2O ligands, forming a hydrogen bond with an amide oxygen of HL (O1W···O9 = 2.828 (3) Å). These channels account for a 21.0% solvent accessible void volume in the structure, as determined by Mercury 4.0.[23] Topologically, GUF-3(Ln) is related to GUF-2(Ln), with greater connectivity due to the coordination of the fourth carboxylate

of HL; it has **(6,3)IIa** topology with point symbol $\{4^8.6^2\}$ (SI, Figure S3).

Whilst it was possible to isolate X-ray quality single crystals of GUF-2(Ln) and GUF-3(Ln) materials (in the case of the Ce(III) congeners, they crystallise alongside one another in solvothermal syntheses) they were challenging to scale up, and it was evident that further phases could form. By slightly modifying the reaction conditions, using a 2.7:1 (*v*/*v*) DMF:H_2O solvent mixture with two equivalents of HNO_3 as modulator, single crystals of GUF-4(Ln) could be isolated for Ln=Ce(III) and Pr(III). GUF-4(Ln) has a similar two-dimensional layered structure to the previous MOFs, but with notable differences in the nature of the layers. The structure of GUF-4(Pr) will be described as representative of the series, and the MOF again crystallises in the *P*-1 space group with a monoprotonated linker. Carrying out the reaction in a more DMF rich solvent mixture seems to have influenced the structure formation, with two coordinated DMF molecules and one coordinated water molecule on each Pr(III), plus an ordered, pore-bound DMF molecule (SI, Figure S4), giving the MOF an overall formula of $([Pr(HL)(DMF)_2(H_2O)]\cdot DMF)_n$. All Pr(III) ions are equivalent, and form a centrosymmetric paddlewheel dimer (Figure 2g) where four carboxylates bridge the two Pr(III) centres in the $\eta_2:\kappa_{1:}\kappa_1$ binding mode, alongside two monodentate carboxylates coordinating in the $\eta_1:\kappa_{1:}\kappa_0$ motif, forming bifurcated hydrogen bonds through their uncoordinated oxygen atoms to adjacent coordinated water molecules (O1W···O7 = 2.658 (6) Å; analogous distances for GUF-4(Ce) are provided in the SI, Table S6) and an amide unit of a neighbouring linker (N1···O7 = 2.976 (6) Å). The coordination sphere of the Pr(III) unit is completed by two *O*-donor DMF ligands, leaving the Pr(III) eight-coordinate, in contrast to the nine-coordinate metal centres in GUF-2(Ln) and GUF-3(Ln). The isophthalate moiety of HL that is doubly deprotonated bridges between clusters to form the two-dimensional sheet structure, while the protonated carboxylic acid unit does not form any significant short contacts, in contrast to GUF-3(Ln) where it coordinated to the metal centres. Viewing the structure down the crystallographic *a*-axis, the sheets of GUF-4(Pr) are stepped (Figure 2h), in comparison to the linear sheets of GUF-2(Ln) and GUF-3(Ln), and there are no notable non-covalent interactions between the sheets. Solvent accessible voids are visible when the structure if viewed down the crystallographic *c*-axis, with a void volume[23] of 42.1% when the DMF guest is removed (Figure 2i). The DMF molecule in the pore forms a bifurcated hydrogen bond (SI, Figure S4) through its formamide oxygen to a proton of the coordinated water molecule (O1W···O3S = 2.867 (6) Å) and an amide proton (N2···O3S = 2.777 (4) Å). With many structural similarities, it is not surprising that GUF-3(Ln) and GUF-4(Ln) display the same underlying **(6,3)IIa** topology, with point symbol $\{4^8.6^2\}$ (SI, Figure S5).

A fourth MOF, GUF-5(Ln), has been characterised by SCXRD where Ln=Ce(III), Pr(III), Nd(III), Sm(III), Eu(III), and Gd(III), with single crystals grown under standard conditions by using 2–10 eq of HNO_3 as a modulator. The only outlier is GUF-5(Ce), where crystals were isolated by modifying the metal:linker ratio to 1:2 and using 10 eq of acetic acid (AcOH) as modulator; the previous three Ce(III) MOFs described required HNO_3 as modulator, suggesting a possible structure directing effect of AcOH. All four Ce(III) MOFs have a Ce(III) to HL ratio of 1:1, which would indicate that the modified reaction stoichiometry is of lesser effect. The isostructural series crystallises in the monoclinic *Cc* space group where the metal atom is nine-coordinate, with three coordinated water ligands, one coordinated DMF, and the linker is again monoprotonated, giving an overall formula of $[Ln(HL)(H_2O)_3(DMF)]_n$. The structure of GUF-5(Nd) will be described here as representative of the series, and any distances reported are tabulated in the supporting information, Table S8, for the other analogues. The MOF consists of one-dimensional chains of crystallographically equivalent Nd(III) ions that project down the crystallographic *c*-axis, which are linked by full isophthalate moieties of HL rather than bridging individual carboxylate moeities; a segment showing two Nd(III) ions is given in Figure 3a. One isophthalate has both carboxylate moieties deprotonated and coordinating in the bidentate $\eta_1:\kappa_{1:}\kappa_1$ motif, while the other has one deprotonated monodentate carboxylate ($\eta_1:\kappa_{1:}\kappa_0$) and one protonated, uncoordinated carboxylate unit that forms hydrogen bonds with a coordinated water ligand (O3W···O5 = 2.854 (4) Å) and an oxy-

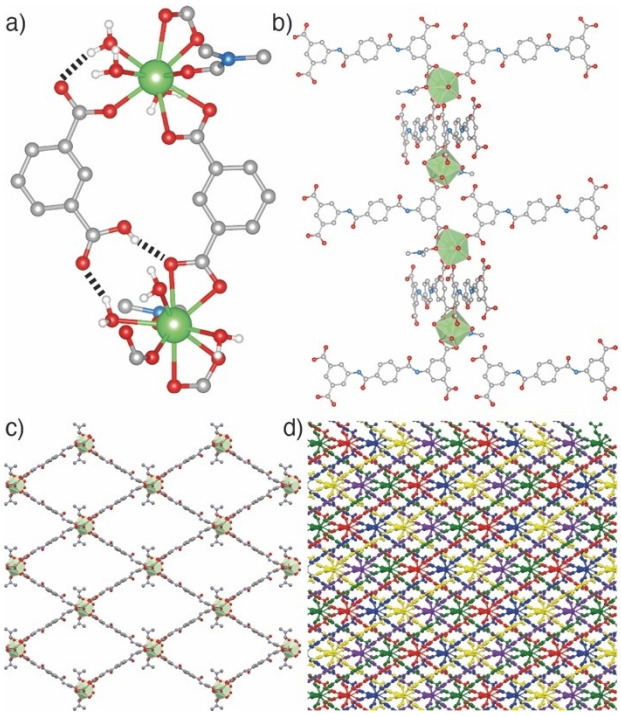

Figure 3. Crystal structure of GUF-5(Nd). a) Connectivity of the crystallographically equivalent Nd(III) ions by fully bridging isophthalate moieties rather than individual bridging carboxylates, with outer sphere hydrogen bonding from a protonated carboxylic acid group. b) Projection of HL^{3-} linkers from the one-dimensional chain SBU. c) Diamondoid channels of a single net of GUF-5(Nd) viewed down the crystallographic *c*-axis. Nd: green; C: grey; O: red; N: blue; H: white. H atoms removed for clarity other than those involved in outer sphere H-bonding interactions in part a). d) Five-fold interpenetration, with each net coloured differently, also viewed down the crystallographic *c*-axis.

gen atom of a bidentate carboxylate (O6···O2 = 2.548 (4) Å). A further outer sphere hydrogen bond is evident between the non-coordinated oxygen atom of the monodentate carboxylate and a second coordinated water ligand (O2W···O8 = 2.665 (3) Å), contrasting both GUF-3(Ln), where the protonated carboxylate coordinates, and GUF-4(Ln), where it forms no significant short contacts. The coordination sphere of the Nd(III) ions is therefore composed of two bidentate carboxylates, one monodentate carboxylate, three water molecules and one DMF molecule.

Linker molecules project from the chains in a staggered fashion (Figure 3b) to form diamond shaped nets with significant channels down the crystallographic *c*-axis (Figure 3c), sufficient to facilitate five-fold interpenetration (Figure 3d). The densely packed structure contains a number of inter-net hydrogen bonds. One water ligand hydrogen bonds to an amide oxygen (O1W···O10 = 2.871 (3) Å) and carboxylate oxygen (O1W···O8 = 2.784 (3) Å) of the same linker, there are similar water to amide (O2W···O9 = 2.817 (3) Å) and water to carboxylate (O3W···O4 = 2.978 (3) Å) interactions with the other ligands, while an amide proton hydrogen bonds to a bidentate carboxylate (N1···O3 = 2.918 (3) Å). Topological analysis confirms that GUF-5(Ln) displays a three-connected unimodal net with **ths** topology (SI, Figure S6) that exhibits class **Ia** (Z = 5) interpenetration (Figure 3d) and point symbol $\{10^3\}$.

Crystal structures of GUF-6(Ln), where Ln=Sm(III), Eu(III), and Gd(III), were obtained from syntheses under standard conditions with 10 eq of benzoic acid as modulator. It was also possible to isolate crystals of the MOFs where Ln=Tb(III), Ho(III), and Er(III) by using HNO_3 modulation and tuning the solvent system, but the diffraction data were only sufficient to refine unit cell parameters that confirm formation of the GUF-6(Ln) structure. In contrast to the previous MOFs, GUF-6(Ln) displays a fully deprotonated linker with a different metal:linker stoichiometry to ensure charge balance; the overall formula is $([Ln_2(L)_{1.5}(H_2O)_3]\cdot H_2O)_n$. The structure of GUF-6(Eu) will be described here, which crystallises in the *C2/c* space group and contains two crystallographically independent, eight-coordinate Eu(III) ions that form dimers (Figure 4a). One metal ion (Eu1) is bound entirely by carboxylate oxygen atoms; four of the oxygen donors come from two $\eta_1{:}\kappa_{1:}\kappa_1$ carboxylates of two adjacent ligands, while two $\eta_2{:}\kappa_{1:}\kappa_1$ carboxylates bridge the two lanthanide ions of the dimer. A third carboxylate bridges with a $\eta_2{:}\kappa_{1:}\kappa_2$ motif to provide one O-donor, and the final oxygen comes from a carboxylate that bridges to an adjacent dimer in a $\eta_2{:}\kappa_{1:}\kappa_1$ motif, resulting in a one-dimensional chain SBU. The other metal ion (Eu2) is bound by two oxygen donors from the $\eta_2{:}\kappa_{1:}\kappa_1$ carboxylates bridging across the dimer, two oxygen donors from the bridging $\eta_2{:}\kappa_{1:}\kappa_2$ carboxylate, a single O-donor from the $\eta_2{:}\kappa_{1:}\kappa_1$ carboxylate that bridges adjacent dimers, and three water ligands. One of the water molecules coordinated to Eu2 forms outer sphere hydrogen bonds to carboxylates from two symmetry independent linkers that are coordinated to the adjacent Eu1 (O2W···O8 = 2.677 (5) Å, O2W···O11 = 2.874 (6) Å; distances for other congeners given in the SI, Table S10). There are two crystallographically independent linker molecules. The isophthalate units of one linker further connect the Eu(III) dimers along the chain – each carboxylate of the isophthalate connecting adjacent dimers – while another carboxylate bridges the dimer in a $\eta_2{:}\kappa_{1:}\kappa_1$ motif (Figure 4b). These L^{4-} units form off-set stacked dimers at a distance of approximately 4.1 Å apart. The second linker, which is centred on an inversion centre, is disordered at its central terephthaloyl moiety and is also associated with a positionally disordered pore-bound water molecule, but connects adjacent chain SBUs that run down the crystallographic *b*-axis to form the three-dimensional net (Figure 4c). The resulting structure is reminis-

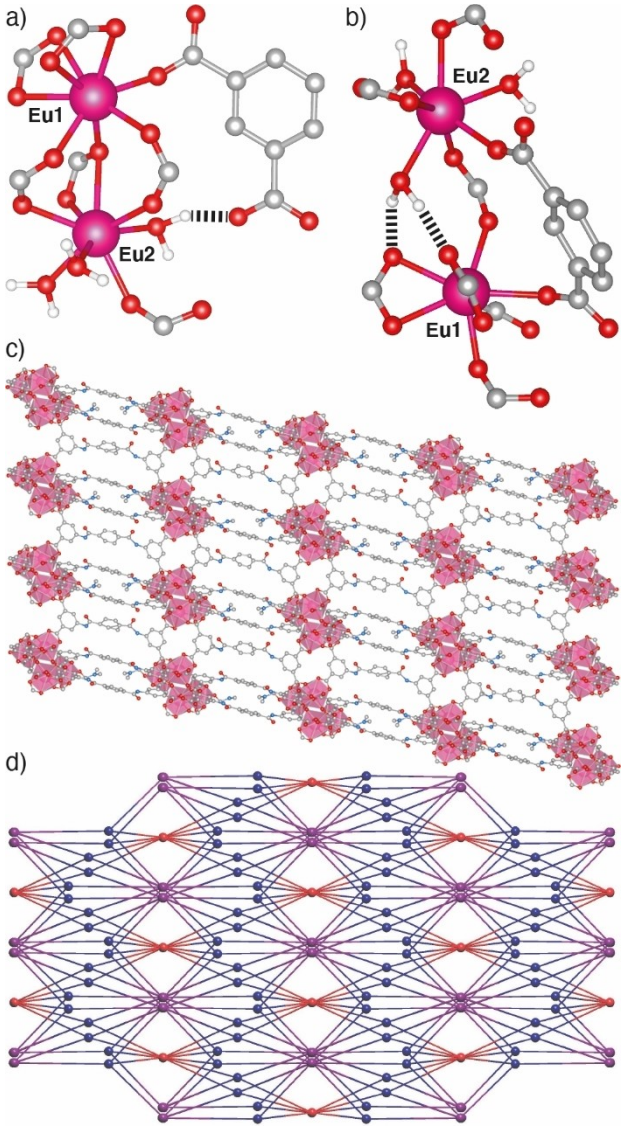

Figure 4. Solid state structure of GUF-6(Eu). a) Bridged lanthanide dimer stabilised by outer sphere hydrogen bonding. b) Connection of these dimers into a one-dimensional chain SBU, with further outer sphere hydrogen bonding (the H-bond in part a) is also represented in part b)). c) Packing structure viewed down the crystallographic *b*-axis. Eu: deep pink; C: grey; O: red; N: blue; H: white. H atoms removed for clarity other than those involved in outer sphere H-bonding interactions in parts a) and b). Linker disorder removed for clarity. d) Topological representation of GUF-6(Eu) viewed down the crystallographic *c*-axis.

cent of the previously reported $[Ln_2(L)_{1.5}(DMF)_4]_n$ materials,[20] but with differences in the SBU (1D chain vs discrete dimers), coordinated solvent (three water ligands on one Ln(III) only vs two DMF ligands on each Ln(III)), and topology. Topologically, GUF-6(Ln) is a 4 nodal, 4,6,6,7-connected net with $(4\text{-c})_2(6\text{-c})(6\text{-c})_2(7\text{-c})_2$ stoichiometry and has a previously unobserved topology type (Figure 4d) where the point symbol was calculated to be $\{4^{11}.6^9.8\}_2\{4^5.6\}_2\{4^6.6^6.8^3\}\{4^8.6^7\}_2$.

Crystals of GUF-7(Ln) can be isolated where Ln=Tb(III), Dy(III), Ho(III), Er(III), and Yb(III) using HNO_3 modulation; this MOF crystallises in the $P2_1/n$ space group where the Ln(III) atom is eight-coordinate. The MOFs were crystallised under standard conditions except for GUF-7(Yb), which required nearly pure DMF as solvent and reaction temperatures of 120 °C. In GUF-7(Ln), the ligand is once again monoprotonated, with two coordinated water ligands giving an overall formula of $[Ln(HL)(H_2O)_2]_n$. The crystal structure of GUF-7(Yb) is described here, with further data for the isostructural analogues provided in the SI, Table S12. Chains of crystallographically equivalent Yb(III) ions running down the crystallographic *a*-axis are bridged by isophthalate units in a centrosymmetric, dimeric motif (Figure 5a). The two equivalent isophthalate units have one bidentate ($\eta_1:\kappa_{1:}\kappa_1$) carboxylate, and a second carboxylate that bridges down the chain in a ($\eta_2:\kappa_{1:}\kappa_1$) motif, forming infinite chains of dimers (Figure 5b). Further interactions down the chain are facilitated by the two coordinated water molecules; both form H-bonds to amide (O1W···O9 = 2.902 (12) Å, O2W···O10 = 2.769 (12) Å) and carboxylate (O1W···O2 = 2.746 (11) Å, O2W···O7 = 2.706 (12) Å) oxygens of a neighbouring ligand. The coordination sphere of the Yb(III) is completed a second bidentate ($\eta_1:\kappa_{1:}\kappa_1$) carboxylate, with the neighbouring carboxylate moiety on this isophthalate being both protonated and uncoordinated, entering into a centrosymmetric carboxylic acid hydrogen bond dimer with an adjacent ligand. The carboxylate is positionally disordered over two sites, leading to four potential H-bond distances across the dimer (O3 A···O4 = 2.51 (4) Å; O3···O4 A = 2.57 (4) Å; O3 A···O4 A = 2.73 (4) Å; O3···O4 = 2.88 (4) Å). This leads to significant channels down the *a*-axis, with a solvent accessible void volume[23] of 34.0% (Figure 5c). GUF-7(Ln) is therefore a three-dimensional, non-interpenetrated structure with **sra** topology (SI, Figure S8).

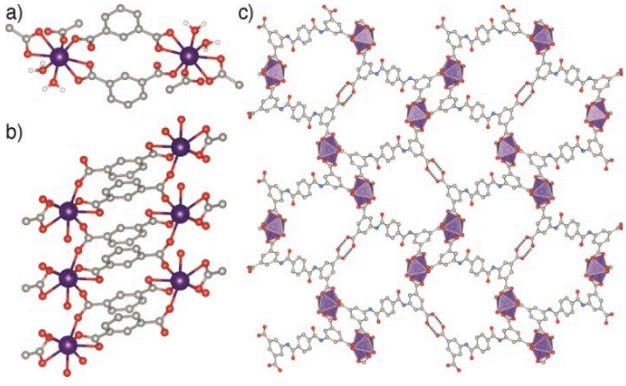

Figure 5. Crystal structure of GUF-7(Yb). a) Isophthalate bridged dimers of Yb(III) ions. b) Connection of these dimers by bridging carboxylate units into one-dimensional chain SBUs that run down the crystallographic *a*-axis. c) Packing structure viewed down the crystallographic *a*-axis, showing formation of carboxylate H-bond dimers and large solvent accessible channels. Yb: purple; C: grey; O: red; N: blue; H: white. Disorder and H atoms removed for clarity other than protons on coordinated water ligands in part a).

These six MOFs exhibit some common features but also topological diversity as a consequence of the versatile coordination chemistry of the lanthanides and also the flexibility of the bis-amide linker. This is evident in the linker adopting both *syn* and *anti* conformations with respect to the two amide moieties across the structures, and deviating from co-planarity of the aromatic rings (see SI, Section S4). These features also make control over phase formation challenging. Whilst it is clear that the ionic radii of the lanthanides play a key role in structure direction – GUF-2(Ln), GUF-3(Ln) and GUF-5(Ln) have nine-coordinate lanthanide ions while GUF-4(Ln), GUF-6(Ln) and GUF-7(Ln) have eight coordinate lanthanide ions – there are examples where crystals of different phases can be formed from the same metal-ligand combination, influenced by the reaction conditions and potentially modulator. As such, modulated self-assembly[13] was used to attempt to isolate phase pure bulk samples and extend the incidence of the individual phases to additional lanthanides, by utilising both mineral acids to control pH, and monotopic carboxylic acids that can enhance the crystallinity and phase purity of the MOFs, as well as modulate the pH. During these studies it was found that isolation of phase pure samples of GUF-2(Ln), GUF-3(Ln) and GUF-4(Ln) was highly challenging, and it was not possible to scale up phase pure samples.

Bulk Powder Samples

During the identification of the different phases above, HNO_3 was by far the most successful modulator in producing X-ray quality single crystals for structural analysis. In the first instance, attempts to scale up samples (SI, Section S5) therefore relied on a modulator screen, using five equivalents of modulator relative to the amount of metal nitrate. This was carried out in the synthesis of Gd(III) and Tb(III) MOFs of the ligand, with these lanthanides selected due to their intermediary position in the *f*-block suggesting potential access to multiple phases. Isolated solids were subsequently characterised by powder X-ray diffraction (PXRD), using predicted diffractograms generated from the single crystal data. Modulator screening (SI, Figures S11 and S12) showed that five equivalents of acetic acid (AcOH) and nitric acid were the most effective at synthesising GUF-5(Gd) and GUF-7(Tb), respectively, as the major products, but they did not yet produce phase pure material. Increasing amounts of AcOH and nitric acid were therefore added to probe the power of modulation, and PXRD analysis subsequently showed that using 20 equivalents each of either AcOH or nitric acid produced phase pure GUF-5(Gd) and GUF-7(Tb), respectively (SI, Figures S13 and S14).

Extending these conditions to other lanthanides, addition of 20 equivalents of AcOH to synthesis containing Ce(III), Pr(III),

Nd(III), or Gd(III) and H_4L led to phase pure GUF-5(Ln) materials. GUF-5(Ln) is also the majority product formed under these conditions with Sm(III) or Eu(III) as the metal, however there is still a minor impurity in these samples, characterised by the presence of a small Bragg peak at $2\theta = 4.8°$, which could not be excluded from the mixture when using different modulators (Figure 6a). Based on the diffractogram predicted from the single crystal structure of GUF-6(Sm) (Figure 6b) this impurity phase likely constitutes GUF-6(Ln). Thermogravimetric analysis (TGA, SI Section S6) also suggests the presence of a phase impurity in the Sm(III) and Eu(III) samples. Qualitatively, the TGA profiles (SI, Figure S18) for these two samples differ from the rest of the GUF-5(Ln) samples where PXRD indicates phase purity. Additionally, the residual masses for the Sm(III) and Eu(III) samples were higher than the others, suggesting a different overall bulk composition.

As the modulator screen did not identify conditions to reliably produce GUF-6(Ln), benzoic acid (BA), which yielded single crystals of the GUF-6(Ln) phases and has also previously been used in the synthesis of Zr MOFs where it aided in the formation of the $Zr_6O_4(OH)_4(RCO_2)_{12}$ cluster,[24] was reinvestigated. Using 10 equivalents of BA relative to the amount of metal nitrate resulted in the synthesis of GUF-6(Ln), as confirmed by PXRD analysis, for syntheses containing Sm(III), Eu(III), or Gd(III) and H_4L (Figure 6b), although some minor additional reflections in the diffractogram for GUF-6(Gd) suggest a minor phase impurity. This was again evident by TGA, as the profile for GUF-6(Gd) differed somewhat from the others (SI, Figure S19). The diffractograms show a large degree of preferred orientation, which can be attributed to the plate like morphology of the GUF-6(Ln) crystals. This method of BA modulation was also tested on the other lanthanide metals, as unit cell analysis showed that the MOF can crystallise with Ln=Tb(III), Ho(III) and Er(III), however, it produced an intractable mixture of phases in all other cases (SI, Figures S15 and S16).

When using 20 equivalents of nitric acid as a modulator in syntheses containing Tb(III), Dy(III), Ho(III), Er(III), Tm(III), Yb(III), or Lu(III) and H_4L, GUF-7(Ln) was formed as the major product, and phase purity was achieved with Tb(III), Dy(III), Ho(III) and Er(III) (Figure 6c). In the syntheses containing Tm(III), Yb(III) and Lu(III), the products showed an impurity phase with Bragg peaks at $2\theta = 6°$ and 11.1°, which could not be removed by using alternative modulators during synthesis. Nevertheless, modulation has extended our knowledge of the presence of the GUF-7(Ln) phase for more lanthanides than those for which single crystals were isolated. It has also been possible to extend the series further and synthesise GUF-7(Gd) as a powder, by using 10 equivalents of dichloroacetic acid (DCA) as a modulator; synthesis of this MOF was not possible when using nitric acid as the modulator (SI, Figure S17). The powder X-ray diffractogram did however contain additional Bragg reflections that likely correspond to unreacted ligand. This preparation of the Gd(III) congener suggests that, as well as having a lanthanide with a suitable ionic radius, the reaction pH is key to preparing GUF-7(Ln), as DCA has a much lower pK_a than the AcOH used to produce GUF-5(Ln). This also correlates with the initial study on HNO_3 modulation of GUF-7(Tb), which required addition of 20 equivalents of modulator to eliminate minor impurities (Figure S14). TGA of the four samples presumed to be phase pure by PXRD showed similar profiles, albeit with slightly differing final mass residues indicating different levels of solvation.

Conclusions

The occurrence of these different Ln(III) MOFs of H_4L has been collated in Figure 7 in the context of the *f*-block elements, for both the single crystal structures described above, and for the samples identified by PXRD. It is clear that the lanthanide ionic radius has a significant structure-directing effect, which has been observed previously in an alternative Ln MOF system,[25] but the phase space is complex, and multiple phases can form from the same metal-ligand combination. Overall, modulated self-assembly has been shown to be applicable to directing structure in lanthanide MOF discovery and synthesis, complementing existing studies with *d*-block MOFs. Modulation has allowed isolation of phase pure materials from the system, directly accessing GUF-5(Ln) by using 20 equivalents of AcOH as modulator, GUF-6(Ln) by using 10 equivalents of benzoic acid, and GUF-7(Ln) by using 20 equivalents of HNO_3, all as bulk powders. The appropriate choice of modulator (2–4 equivalents of HNO_3) has also allowed characterisation of GUF-2(Ln), GUF-3(Ln) and GUF-4(Ln), with crystals of the latter favoured by

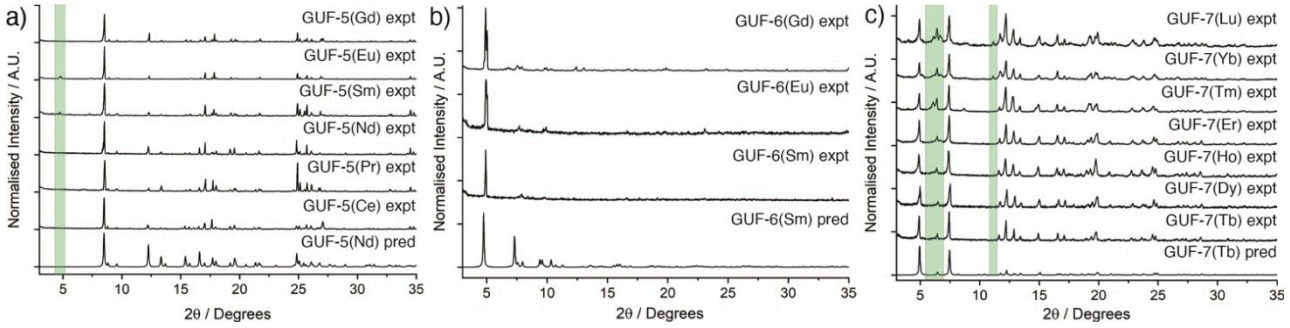

Figure 6. Stacked powder X-ray diffractograms of bulk samples of Ln MOFs of L prepared by modulated self-assembly, using a) 20 equiv. acetic acid, b) 10 equiv. benzoic acid, and c) 20 equiv. nitric acid as modulators of solvothermal syntheses.

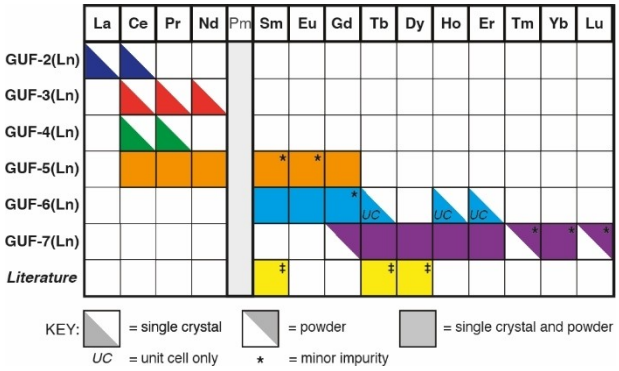

Figure 7. Overview of the known Ln(III) MOFs of H_4L by lanthanide, collated in terms of their appearance in the *f*-block and the form in which they have been characterised (single crystal structure only, bulk powder only, or both). ‡Literature structures reported in refs [20a] and [20b].

increasing the DMF content of reactions, but is yet to offer scale-up. Solvent therefore clearly can influence phase formation, which is further evidenced by the additional phase that has previously been reported for H_4L MOFs linked by Sm(III), Tb(III), and Dy(III). These myriad factors, combined with the flexibility of Ln coordination chemistry and the propensity for H_4L to adopt multiple different co-conformations in the solid state, suggests that other phases in this lanathanide-ligand system remain to be discovered.

Acknowledgements

R.S.F. thanks the Royal Society for receipt of a URF, and the University of Glasgow and EPSRC (EP/N509668/1) for funding.

Conflict of Interest

The authors declare no conflict of interest.

Data Availability Statement

The data that support the findings of this study are openly available in University of Glasgow, Enlighten repository at https://doi.org/10.5525/gla.researchdata.1319, reference number 1319.

Keywords: metal-organic frameworks · coordination modulation · lanthanides · self-assembly · flexible

[1] H. Furukawa, K. E. Cordova, M. O'Keeffe, O. M. Yaghi, *Science* **2013**, *341*, 1230444.
[2] a) M. Li, S. Gul, D. Tian, E. Zhou, Y. Wang, Y. Han, L. Yin, L. Huang, *Dalton Trans.* **2018**, *47*, 12868–12872; b) C. Liu, B. Yan, *New J. Chem.* **2015**, *39*, 1125–1131; c) H. S. Quah, W. Chen, M. K. Schreyer, H. Yang, M. W. Wong, W. Ji, J. J. Vittal, *Nat. Commun.* **2015**, *6*, 7954; d) H. S. Quah, V. Nalla, K. Zheng, C. A. Lee, X. Liu, J. J. Vittal, *Chem. Mater.* **2017**, *29*, 7424–7430.
[3] a) R. Li, S.-H. Wang, Z.-F. Liu, X.-X. Chen, Y. Xiao, F.-K. Zheng, G.-C. Guo, *Cryst. Growth Des.* **2016**, *16*, 3969–3975; b) D. F. Sava, L. E. S. Rohwer, M. A. Rodriguez, T. M. Nenoff, *J. Am. Chem. Soc.* **2012**, *134*, 3983–3986; c) J. Park, M. Oh, *CrystEngComm* **2016**, *18*, 8372–8376; d) Y. Gai, Q. Guo, K. Xiong, F. Jiang, C. Li, X. Li, Y. Chen, C. Zhu, Q. Huang, R. Yao, M. Hong, *Cryst. Growth Des.* **2017**, *17*, 940–944; e) T. Song, G. Zhang, Y. Cui, Y. Yang, G. Qian, *CrystEngComm* **2016**, *18*, 8366–8371.
[4] a) D. Yue, D. Zhao, J. Zhang, L. Zhang, K. Jiang, X. Zhang, Y. Cui, Y. Yang, B. Chen, G. Qian, *Chem. Commun.* **2017**, *53*, 11221–11224; b) Z.-J. Li, X.-Y. Li, Y.-T. Yan, L. Hou, W.-Y. Zhang, Y.-Y. Wang, *Cryst. Growth Des.* **2018**, *18*, 431–440; c) H. Xu, X. Rao, J. Gao, J. Yu, Z. Wang, Z. Dou, Y. Cui, Y. Yang, B. Chen, G. Qian, *Chem. Commun.* **2012**, *48*, 7377–7379; d) Y.-M. Zhu, C.-H. Zeng, T.-S. Chu, H.-M. Wang, Y.-Y. Yang, Y.-X. Tong, C.-Y. Su, W.-T. Wong, *J. Mater. Chem. A* **2013**, *1*, 11312–11319; e) Q. Zhang, J. Wang, A. M. Kirillov, W. Dou, C. Xu, C. Xu, L. Yang, R. Fang, W. Liu, *ACS Appl. Mater. Interfaces* **2018**, *10*, 23976–23986; f) Y. Zhang, S. Yuan, G. Day, X. Wang, X. Yang, H.-C. Zhou, *Coord. Chem. Rev.* **2018**, *354*, 28–45; g) Y. Liu, X.-Y. Xie, C. Cheng, Z.-S. Shao, H.-S. Wang, *J. Mater. Chem. C* **2019**, *7*, 10743–10763.
[5] a) X. Li, S. Lu, D. Tu, W. Zheng, X. Chen, *Nanoscale* **2020**, *12*, 15021–15035; b) X. Li, S. Zhou, S. Lu, D. Tu, W. Zheng, Y. Liu, R. Li, X. Chen, *ACS Appl. Mater. Interfaces* **2019**, *11*, 43989–43995; c) F. Demir Duman, R. S. Forgan, *J. Mater. Chem. B* **2021**, *9*, 3423–3449.
[6] a) P. Cheng, *Lanthanide Metal-Organic Frameworks*, 1st ed., Springer-Verlag Berlin Heidelberg, **2015**; b) F. Saraci, V. Quezada-Novoa, P. R. Donnarumma, A. J. Howarth, *Chem. Soc. Rev.* **2020**, *49*, 7949–7977.
[7] J.-C. G. Bünzli, C. Piguet, *Chem. Soc. Rev.* **2005**, *34*, 1048–1077.
[8] a) Y. Cui, B. Chen, G. Qian, *Coord. Chem. Rev.* **2014**, *273–274*, 76–86; b) T. Sun, Y. Gao, Y. Du, L. Zhou, X. Chen, *Front. Chem.* **2021**, *8*, 624593; c) S.-N. Zhao, G. Wang, D. Poelman, P. Van Der Voort, *Materials* **2018**, *11*, 572; d) B. Yan, *Acc. Chem. Res.* **2017**, *50*, 2789–2798; e) D. Hu, Y. Song, L. Wang, *J. Nanopart. Res.* **2015**, *17*, 310.
[9] J.-C. G. Bünzli, *J. Coord. Chem.* **2014**, *67*, 3706–3733.
[10] C. Pagis, M. Ferbinteanu, G. Rothenberg, S. Tanase, *ACS Catal.* **2016**, *6*, 6063–6072.
[11] Y. Kitamura, E. Terado, Z. Zhang, H. Yoshikawa, T. Inose, H. Uji-i, M. Tanimizu, A. Inokuchi, Y. Kamakura, D. Tanaka, *Chem. Eur. J.* **2021**, *27*, 16347–16353.
[12] a) T. M. Reineke, M. Eddaoudi, M. Fehr, D. Kelley, O. M. Yaghi, *J. Am. Chem. Soc.* **1999**, *121*, 1651–1657; b) Y. Han, X. Li, L. Li, C. Ma, Z. Shen, Y. Song, X. You, *Inorg. Chem.* **2010**, *49*, 10781–10787; c) H. He, H. Ma, D. Sun, L. Zhang, R. Wang, D. Sun, *Cryst. Growth Des.* **2013**, *13*, 3154–3161; d) H. He, D. Yuan, H. Ma, D. Sun, G. Zhang, H.-C. Zhou, *Inorg. Chem.* **2010**, *49*, 7605–7607; e) T. M. Reineke, M. Eddaoudi, M. O'Keeffe, O. M. Yaghi, *Angew. Chem. Int. Ed.* **1999**, *38*, 2590–2594; *Angew. Chem.* **1999**, *111*, 2712–2716; f) E. Neofotistou, C. D. Malliakas, P. N. Trikalitis, *CrystEngComm* **2010**, *12*, 1034–1037; g) X.-L. Lv, L. Feng, K.-Y. Wang, L.-H. Xie, T. He, W. Wu, J.-R. Li, H.-C. Zhou, *Angew. Chem. Int. Ed.* **2021**, *60*, 2053–2057; *Angew. Chem.* **2021**, *133*, 2081–2085; h) X.-L. Lv, L. Feng, L.-H. Xie, T. He, W. Wu, K.-Y. Wang, G. Si, B. Wang, J.-R. Li, H.-C. Zhou, *J. Am. Chem. Soc.* **2021**, *143*, 2784–2791.
[13] R. S. Forgan, *Chem. Sci.* **2020**, *11*, 4546–4562.
[14] F. J. Carmona, C. R. Maldonado, S. Ikemura, C. C. Romão, Z. Huang, H. Xu, X. Zou, S. Kitagawa, S. Furukawa, E. Barea, *ACS Appl. Mater. Interfaces* **2018**, *10*, 31158–31167.

[15] a) D. Bara, E. G. Meekel, I. Pakamorė, C. Wilson, S. Ling, R. S. Forgan, *Mater. Horiz.* **2021**, *8*, 3377–3386; b) D. Bara, C. Wilson, M. Mörtel, M. M. Khusniyarov, S. Ling, B. Slater, S. Sproules, R. S. Forgan, *J. Am. Chem. Soc.* **2019**, *141*, 8346–8357.
[16] L. Yang, T. Zhao, I. Boldog, C. Janiak, X.-Y. Yang, Q. Li, Y.-J. Zhou, Y. Xia, D.-W. Lai, Y.-J. Liu, *Dalton Trans.* **2019**, *48*, 989–996.
[17] a) A. K. Pereira Leite, B. S. Barros, J. Kulesza, J. F. Silva do Nascimento, D. Maria de Araújo Melo, A. Anderson Silva de Oliveira, *Mater. Res.* **2017**, *20*, 681–687; b) H. Guo, Y. Zhu, S. Wang, S. Su, L. Zhou, H. Zhang, *Chem. Mater.* **2012**, *24*, 444–450; c) G. Arroyos, R. C. G. Frem, *CrystEngComm* **2020**, *22*, 2439–2446; d) G. E. Gomez, M. C. Bernini, E. V. Brusau, G. E. Narda, D. Vega, A. M. Kaczmarek, R. Van Deun, M. Nazzarro, *Dalton Trans.* **2015**, *44*, 3417–3429; e) Z. W. Jiang, Y. C. Zou, T. T. Zhao, S. J. Zhen, Y. F. Li, C. Z. Huang, *Angew. Chem. Int. Ed.* **2020**, *59*, 3300–3306; *Angew. Chem.* **2020**, *132*, 3326–3332.
[18] S. L. Griffin, C. Wilson, R. S. Forgan, *Front. Chem.* **2019**, *7*, 36.
[19] G. S. Silva, J. D. L. Dutra, N. B. da Costa, S. Alves, R. O. Freire, *J. Phys. Chem. A* **2020**, *124*, 7678–7684.
[20] a) R. Yun, Y. Jiang, H. Wu, S. Luo, *J. Coord. Chem.* **2016**, *69*, 3303–3308; b) Q. Lin, W. Xie, Z. Zong, Z. Liu, Y. Sun, L. Liang, *New J. Chem.* **2021**, *45*, 7382–7389.
[21] P. J. Kitson, R. J. Marshall, D. Long, R. S. Forgan, L. Cronin, *Angew. Chem. Int. Ed.* **2014**, *53*, 12723–12728; *Angew. Chem.* **2014**, *126*, 12937–12942.
[22] a) J. Luo, J.-W. Wang, J.-H. Zhang, S. Lai, D.-C. Zhong, *CrystEngComm* **2018**, *20*, 5884–5898; b) R.-B. Lin, Y. He, P. Li, H. Wang, W. Zhou, B. Chen, *Chem. Soc. Rev.* **2019**, *48*, 1362–1389; c) B. Wang, R.-B. Lin, Z. Zhang, S. Xiang, B. Chen, *J. Am. Chem. Soc.* **2020**, *142*, 14399–14416; d) P. Li, M. R. Ryder, J. F. Stoddart, *Acc. Mater. Res.* **2020**, *1*, 77–87.
[23] C. F. Macrae, I. Sovago, S. J. Cottrell, P. T. A. Galek, P. McCabe, E. Pidcock, M. Platings, G. P. Shields, J. S. Stevens, M. Towler, P. A. Wood, *J. Appl. Crystallogr.* **2020**, *53*, 226–235.
[24] A. Schaate, P. Roy, A. Godt, J. Lippke, F. Waltz, M. Wiebcke, P. Behrens, *Chem. Eur. J.* **2011**, *17*, 6643–6651.
[25] H. Ya Gao, W. Li Peng, P. Pan Meng, X. Feng Feng, J. Qiang Li, H. Qiong Wu, C. Sheng Yan, Y. Yang Xiong, F. Luo, *Chem. Commun.* **2017**, *53*, 5737–5739.

Manuscript received: May 12, 2022
Revised manuscript received: June 23, 2022
Accepted manuscript online: July 11, 2022

